Article :Dispersion atmosphérique via une approche lagrangienne stochastique application à une zone urbaine idéalisée sous des conditions météorologiques neutre et stable

Cet article a été soumis à *International Journal of Wind Engineering and Industrial Aerodynamics*. Nous y proposons de valider le modèle lagrangien stochastique SLM sur une campagne expérimentale impliquant des obstacles : la campagne MUST (*Mock Urban Setting Test*), conduite dans le désert de l'Utah aux Etats-Unis en 2001. Dans un premier temps, nous décrivons la campagne expérimentale, puis nous exposons les résultats des simulations réalisées. Nous comparons le modèle lagrangien étudié aux méthodes eulériennes ainsi qu'aux mesures de l'expérience. Un point important soulevé dans cet article est qu'il s'agit de garder à l'esprit les différences théoriques impliquées par les différents modèles eulérien et lagrangien (notamment au niveau de l'ordre de fermeture turbulente) afin d'être à même de mener des analyses critiques des résultats de simulations.

Sommaire

7.1 Article **161**

7.2 Complément **191**

7.1 Article

Atmospheric dispersion using a Lagrangian stochastic approach: application to an idealized urban area under neutral and stable meteorological conditions

Meïssam L. Bahlali[a], Eric Dupont[a], Bertrand Carissimo[a]

[a] *CEREA, Joint laboratory Ecole des Ponts ParisTech/EDF R&D, 6 quai Watier, 78401 Chatou Cedex, France*

Abstract

We present an adaptation of the Lagrangian dispersion module of the computational fluid dynamics (CFD) open source code *Code_Saturne* (`http://code-saturne.org/`) to simulate atmospheric dispersion of pollutants in complex urban geometries or around industrial plants. The wind is modeled within the same code with an Eulerian RANS (Reynolds-averaged Navier-Stokes equations) approach and thus involves the solution for the ensemble-mean velocity field and turbulent moments, using first-order $k-\epsilon$ or second-order $R_{ij}-\epsilon$ turbulence closures adapted to the atmosphere and complex geometries.

The Lagrangian stochastic model used for the dispersion of the particles within this flow field is the simplified Langevin model of Pope (2000), an approach referred to as PDF (Probability Density Function) method. This formulation of model has not been widely used in atmospheric applications, despite interesting theoretical and computational benefits. Therefore, its usage must be validated on different atmospheric cases. In this paper, we present the validation of the model with a field experiment, considering atmospheric stratification and buildings: the MUST (Mock Urban Setting Test) campaign, conducted in Utah's desert, USA.

Keywords: Atmospheric dispersion, Lagrangian models, Eulerian models, Wind flow modeling, MUST experiment

1. Introduction

An atmospheric dispersion model is a tool that can be used to simulate the atmospheric phenomena involved in the turbulent pollutant dispersion process. The differences between the many existing models to date are mainly in terms of the number of atmospheric processes considered, their degree of complexity, their field of application and, in particular, the methods used to solve the equations governing them. We can distinguish mainly three types of models:

Email address: `meissambahlali@gmail.com` (Meïssam L. Bahlali)

- Gaussian models, based on the analytical resolution of the so-called advection-diffusion equation (on a scalar corresponding to the concentration of pollutant) coupled with semi-empirical parameterizations of the main physical phenomena;
- Eulerian models, based on the resolution of the discretized advection-diffusion equation in time and space on a mesh;
- Lagrangian models, based on the computation of particle trajectories.

Eulerian models, when used through Computational Fluid Dynamics (CFD) methods, rely on the resolution of the advection-diffusion equation of a scalar on a mesh. This equation implies the knowledge of the velocity and turbulent fields. Therefore, the first step is the resolution of the Eulerian Navier-Stokes momentum equation, in order to compute the flow in which the dispersion will then take place. Generally, the resolution of the Navier-Stokes momentum and scalar transport equations are carried out within the same model. This therefore supposes to have a model that provides a solution for the dynamical fields of good enough quality, since it would strongly influence the solution obtained for the concentration field calculated through the advection-diffusion equation. In particular, this highlights the crucial importance of a correct modeling of flow turbulence.

On the other hand, Lagrangian models consist of calculating and following the trajectories of particles in a turbulent flow. Thus, the frame of reference is not fixed but follows the cloud described by a large number of particles emitted into the atmosphere. For each of these particles, a stochastic differential equation of a Langevin type is written on their velocity. By integrating over time, we are thus able to get the position of each and then deduce the concentration field over the computational domain. The main strength of Lagrangian models is that they treat convection without any approximation. In particular, they can treat without approximation local source terms when they are provided as known expressions of the variables associated with the particles, such as chemical source terms (Minier, 2015). Also, Lagrangian models are grid-free, which makes them accurate to capture the different turbulent structures in a statistical sense and avoid numerical diffusion problems that can be encountered within Eulerian models – especially near the source. However, one must keep in mind that they usually still depend on a grid in two ways:

- the stochastic differential equation that governs the velocity evolution of the particles usually involves fluid mean quantities that are provided by a grid-based meteorological pre-processor or a CFD calculation;
- the concept of 'concentration' is by definition mesh-based.

Both CFD Eulerian and Lagrangian models are well-suited for atmospheric dispersion studies in urban neighborhoods or around industrial plants, in the sense that they are capable to capture the complex interactions between the air flow and the buildings for different meteorological conditions. However, these two types of models have often been compared ignoring the level of turbulence closure used for each. Loosely speaking, a

common belief is that 'Eulerian models do not work well near the source'. In reality, the correct affirmation would be: 'Eulerian first-order models, based on a gradient-diffusion hypothesis, do not work well near the source', since this region corresponds to the short-time limit where the fully diffusive regime has not been reached yet (Taylor, 1921). In fact, in the atmospheric dispersion field, when we refer to Lagrangian models, it is usually to models simulating the particle **velocities** as stochastic diffusion processes, which by construction makes them second-order. On the other hand, a Lagrangian model simulating the **positions** as stochastic diffusion processes is first-order and would thus be equivalent to an Eulerian model using a gradient-diffusion hypothesis. More details can be found on that subject in Minier (2016). To sum up, the Eulerian/Lagrangian comparisons should not be about the approaches in themselves but rather about the level of closure that is considered. Throughout this paper, we will be coming back on this point of significant importance when it comes to rigorously comparing the accuracy of the results given by both approaches.

In the past few years, the constantly increasing computing power has enabled (and above all made easier) the use of Lagrangian stochastic methods for atmospheric purposes – see for example Franzese (2003), Stohl et al. (2005), Cassiani et al. (2005a,b), Bernardin et al. (2009), Alessandrini and Ferrero (2009), Tinarelli et al. (2013), etc. For our work, a simulation tool using a Lagrangian PDF (Probability Density Function) to carry out pollutant dispersion studies has been developed in the three-dimensional CFD code *Code_Saturne* (`http://code-saturne.org/`, see Archambeau et al. (2004) for more details). It has been validated on simple academic cases and showed to satisfactorily respect the well-mixed condition (see Bahlali et al. (2018a,b)). This paper is concerned with validating the model in real conditions by studying continuous point source dispersion of a non-reactive pollutant in an idealized urban area, as such a case is typical of an industrial or accidental release.

The present work will focus on the Mock Urban Setting Test (MUST) campaign, which has been widely studied in the literature. For previous numerical simulations of the experiment, the reader may for example refer to Hanna et al. (2004), Camelli et al. (2005), Donnelly et al. (2009), Antonioni et al. (2012), Kumar et al. (2015). Comparisons between different modeling systems have also been studied: Santiago et al. (2010) and Dejoan et al. (2010) compared large-eddy simulations (LES) to Reynolds-averaged Navier-Stokes (RANS) computations, and Castelli et al. (2017) performed comparisons between different atmospheric Eulerian and Lagrangian modeling approaches. Experimental comparisons have been conducted as well: Leitl et al. (2007) worked on the Hamburg wind tunnel experiment, Yee et al. (2006) compared experimental wind-tunnel and water-channel simulations.

In the CFD code *Code_Saturne*, previous numerical simulations of the MUST campaign have also already been performed by Milliez and Carissimo (2007, 2008) and used an Eulerian first-order model of turbulent dispersion. The present work aims at studying the same cases using the Lagrangian stochastic model. The objective is twofold:

- first, we would like to assess the accuracy of the results provided by the Lagrangian model for this specific industrial application;
- second, we would like, in the same CFD simulations, to compare the Lagrangian results to the ones obtained with several Eulerian turbulence models, and above all explain the differences to provide a better understanding of the different modeling options.

A specificity of this work is that the wind is modeled *within the same code* as the dispersion, with an Eulerian RANS approach. It thus involves the solution for the ensemble-mean velocity field and turbulent moments, using first-order $k-\epsilon$ or second-order $R_{ij}-\epsilon$ turbulence closures adapted to the atmosphere and complex geometries. Note that Milliez and Carissimo (2007, 2008) only simulated the wind dynamical mean fields using a $k-\epsilon$ model. Therefore, in addition to the Lagrangian results, this paper will also expose new results on the Eulerian approach through the use of the second-order $R_{ij}-\epsilon$ model for the wind mean quantities.

This paper will be organized as follows. First, we will introduce both the Eulerian and Lagrangian model equations used in this work. Second, we will expose the experiment characteristics and the two cases we have chosen to study. Finally, we will show results for both these cases and the different modeling approaches will be discussed.

2. Model equations

The methodology for atmospheric dispersion calculations in *Code_Saturne* consists in two simulations:

- the first simulation solves the mean Navier-Stokes equations for the flow field;
- the second simulation restarts from the previous frozen flow field (velocity, turbulence and temperature) and computes the dispersion.

Let us present the different modeling options in Eulerian and Lagrangian approaches.

2.1. The Eulerian approach

Eulerian models, as explained in the introduction, are based on the resolution of the mean advection-diffusion equation of a given Reynolds-averaged scalar $\langle c \rangle$ through its discretization in time and space on a mesh. This equation writes as follows:

$$\frac{\partial \langle c \rangle}{\partial t} + \langle U_j \rangle \frac{\partial \langle c \rangle}{\partial x_j} = \frac{\partial}{\partial x_j} \left(D \frac{\partial \langle c \rangle}{\partial x_j} - \langle U'_{f,j} c' \rangle \right) + \langle S \rangle + \langle R \rangle \ , \tag{1}$$

where $U_{f,j}$ is the fluid velocity along the j axis, D the molecular diffusivity, S and R respectively the source and reactive terms.

This equation involves the unknown term $\langle U'_{f,j} c' \rangle$. For practical applications, two main families of closures are considered:

- first-order models (or algebraic models), which directly provide a local expression for $\langle U'_{f,j}c'\rangle$;
- second-order models, which consist of a complete transport of the turbulent scalar fluxes $\langle U'_{f,j}c'\rangle$.

First-order models are widely used in the atmospheric dispersion literature, usually through the following simple gradient-diffusion hypothesis:

$$\langle U'_{f,j}c'\rangle = -D_t \frac{\partial\langle c\rangle}{\partial x_j} \ , \tag{2}$$

where $D_t = \nu_t/Sc_t$, Sc_t being the turbulent Schmidt number, usually comprised between 0.7 and 1 for air.

In this expression, $\nu_t = C_\mu k^2/\epsilon$ is the fluid turbulent viscosity, k being the turbulent kinetic energy (TKE) and ϵ the turbulent dissipation rate. An important point to recall here is that if a turbulent-viscosity model is used for the resolution of the mean dynamical fields, then obviously, closure of $\langle U'_{f,j}c'\rangle$ will be performed through a first-order model. On the other hand, one can use a second-order $R_{ij}-\epsilon$ model to compute the mean dynamical fields and still use a first-order model for the turbulent scalar fluxes closure (*i.e.*, here, the model of Eq. (2)). Our work will provide new elements on that topic, by comparing, using either a $k-\epsilon$ or a $R_{ij}-\epsilon$ model to compute the mean dynamical fields, the results obtained through a first-order model for the scalar dispersion. As for second-order scalar fluctuations models for meteorological applications, they are in fact still an open and difficult research problem, and the subject of further investigations.

2.2. The Lagrangian approach

Let $\mathbf{X}_p$ be the position of a particle included in the air flow and $\mathbf{U}_p$ its velocity. Both variables are driven by the following system:

$$dX_{p,i} = U_{p,i}(t)dt \ , \tag{3a}$$

$$dU_{p,i} = -\frac{1}{\rho}\frac{\partial\langle P\rangle}{\partial x_i}dt + (\langle U_{p,i}\rangle - \langle U_{f,i}\rangle)\frac{\partial\langle U_{f,i}\rangle}{\partial x_i} - \frac{U_{p,i}-\langle U_{f,i}\rangle}{T_L}dt + \sqrt{C_0\epsilon}dW_i \ , \tag{3b}$$

where the dW_i are Wiener processes of zero mean and variance dt, and $T_L = \dfrac{1}{\frac{1}{2}+\frac{3}{4}C_0}\dfrac{k}{\epsilon}$ is the Lagrangian integral timescale.

The stochastic differential equation governing the evolution of $\mathbf{U}_p$ is a model inspired by the two-phase flow formulation of Minier and Peirano (2001) and the Simplified Langevin Model (SLM) of Pope (2000) – it actually stands between the two of them, the difference lying in the $(\langle U_{p,i}\rangle - \langle U_{f,i}\rangle)\frac{\partial\langle U_{f,i}\rangle}{\partial x_i}$ term. This formulation makes sense since even though we are dealing with fluid particles (putting us in the single-phase flow situation), particles dispersing from a point source can be seen as a subset of the whole simulated flow.

Therefore, in each cell of the computational domain, their mean velocity has no reason to be equal to the fluid one, hence the non-null production term on the second term of the right-hand-side of Eq. (3b). In fact, for a better understanding, let us assume that the whole flow is represented by particles uniformly distributed in the domain and affect a scalar α to each of them:

$$\begin{cases} \alpha = 1 \text{ if the particle comes from the source;} \\ \alpha = 0 \text{ if it does not come from the source.} \end{cases}$$

Therefore, the condition that the mean particle velocity field needs to observe is: $\mathbf{div}(\alpha\langle\mathbf{U}_p\rangle) = \mathbf{0}$, which is a complete different condition than the one the fluid velocity field has to meet, *i.e.*, $\mathbf{div}(\langle\mathbf{U}_f\rangle) = \mathbf{0}$.

Loosely speaking, this formulation stands in a philosophical line that is close to the LRR-IP (Launder, Reece, Rodi - Isotropization of Production) model of Pope (2000), except that the production term here is related to the mean particle velocity instead of the instantaneous one. This production term actually makes significant physical sense, since it adds more anisotropy to the dispersion of the particles. Furthermore, if we study the limit case of particles modeling the whole flow (*i.e.*, the 'fluid limit'), then it yields $\langle U_{p,i}\rangle = \langle U_{f,i}\rangle$ and the SLM is retrieved. Precisely, Bahlali et al. (2018b) have shown that the SLM fully respects the well-mixed criterion (as defined in Thomson (1987)) and that it is completely consistent with a second-order $R_{ij} - \epsilon$ (Rotta) turbulence model for the fluid phase. Both these conditions are in fact essential for any Lagrangian stochastic model of a Langevin type to be regarded as acceptable (see Minier et al. (2014)). In conclusion, the model defined in Eq. (3), since it relaxes to the SLM for the fluid limit, is well-mixed and able to reproduce transport equations for the first two moments of the velocity field: it can thus reasonably be used to simulate point source dispersion in non-homogeneous flows such as the one we will study in this work. However, one must keep in mind that this model has been developed for neutral conditions. It is possible to use it also for buoyancy-driven flows, as we did in this work, but some improvements can be made for these cases and are the subject of further investigations (cf. conclusion).

It should be noted that this Lagrangian model alone does not take into account molecular diffusion. Indeed, if we add a scalar c to the state vector associated with each particle, then: $dc/dt = 0$ (we deal with conservative particles, with a constant concentration along their trajectories). In order to represent the molecular diffusion phenomenon, a so-called 'micro-mixing model' can be used (see, for example, Villermaux and Devillon (1972); Pope (2000); Sawford (2004); Luhar and Sawford (2005); Amicarelli et al. (2012); Cassiani et al. (2015)). This type of model is often used in the case of reactive pollutants, since in this context molecular diffusion plays an important role. In the case of high Reynolds numbers, molecular diffusion does not affect concentration mean (Pope, 1998), and is therefore generally neglected compared to turbulent diffusion.

3. The Mock Urban Setting Test experiment

3.1. Description of the site

The experimental program this paper focuses on is the Mock Urban Setting Test campaign, conducted in Utah's desert, USA, by the US Defense Threat Reduction Agency (DTRA). It consists of the release of a pollutant in an idealized urban environment represented by several rows of containers. The details of the experiment as well as the results are described in Biltoft (2001) and Yee and Biltoft (2004).

In this work, the objective is to reproduce some of the simulations that have already been performed in the past by Milliez and Carissimo (2007, 2008) in *Mercure* (former name of the atmospheric module of *Code_Saturne*), but completing them with new results using the Lagrangian stochastic model previously introduced and the second-order $R_{ij} - \epsilon$ model for the fluid phase computation. Milliez and Carissimo (2007) described in detail the characteristics of the campaign, which we summarize below:

- 63 emissions of a neutral gas (propylene C_3H_6), among which 58 continuous and 5 puff releases;
- flat terrain with some bushes from 50 cm to 1 m high;
- presence of obstacles through a regular alignment of containers of dimensions 12.2 m (length) $\times$ 2.42 m (width) $\times$ 2.54 m (height);
- different wind conditions through varying angles of incidence, wind velocities, turbulence, temperature, stability conditions;
- different release heights: 0.15 m, 1.3 m, 1.8 m, 2.6 m and 5.2 m.

Figure 1 shows two photos of the MUST experiment. The regular alignment of the containers is supposed to represent an idealized city and the objective of the experiment is to observe the point source dispersion of the propylene continuously released in this environment. We are interested in checking how the Lagrangian model behaves in the presence of obstacles in a real situation. Indeed, when assessing the respect of the well-mixed criterion for the SLM, Bahlali et al. (2018b) studied the case of a non-homogeneous turbulent flow around an obstacle within a boundary layer and observed differences in the behavior of the particles depending on the turbulence model that was used to compute the fluid phase.

The experimental devices used in the campaign are illustrated in Figure 2. Wind and temperature measurements were carried out using sonic anemometers (30-m mast S just upstream the canopy, 32-m central tower T and 8-m masts A, B, C and D inside the canopy). As for pollutant concentrations, they were measured by photoionization detectors (PIDs), positioned on four horizontal lines (*'line 1, 2, 3, 4'* in Figure 2). These four lines were located at height 1.6 m. PIDs were also placed at 6 levels on the masts A, B, C, D and at 8 levels on the tower T.

Figure 1: Some views of the MUST experiment (after Milliez (2006)).

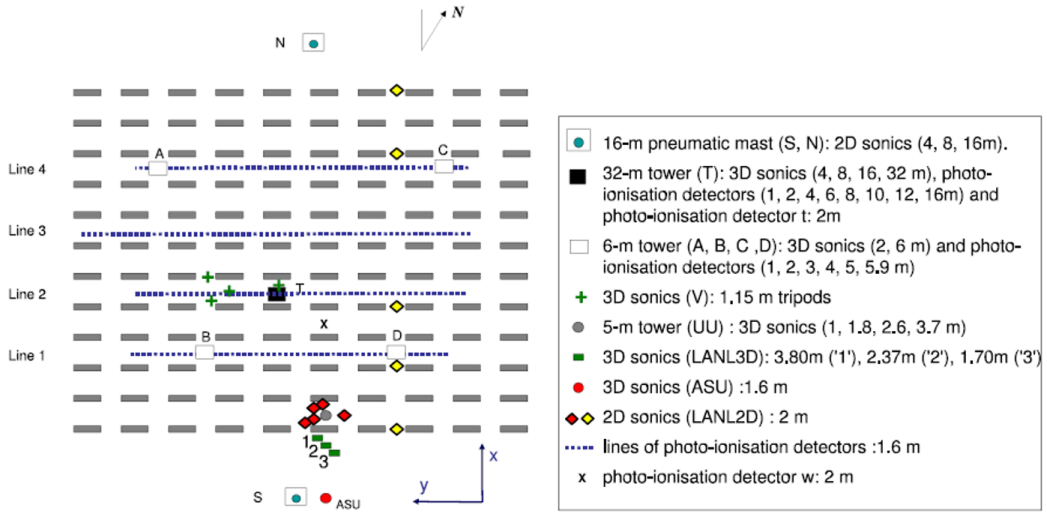

Figure 2: Schematic diagram of the MUST experiment and location of the experimental devices (after Milliez and Carissimo (2008)).

Case	α_4 (deg)	S_4 $(m.s^{-1})$	k_4 $(m^2.s^{-2})$	L (m)	Q $(L.min^{-1})$	Source location	z_s (m)
2681829	-41	7.93	4.263	28000	225	29	1.8
2692157	43	2.98	0.510	130	225	36	2.6

Table 1: Characteristics of the two selected trials: S_4 and α_4 are respectively the mean wind horizontal speed and direction at the 4-m level of mast S, k_4 is the turbulent kinetic energy and L the Monin-Obukhov length at the 4-m level of tower T, Q is the tracer release rate at the source, 'Source location' is the position of the source and z_s is the height of the source (after Milliez and Carissimo (2007)).

Finally, it should be noted that the tracer releases occured at dusk or dawn, thus under meteorological conditions ranging from stable to neutral. The duration of each release was 15 min and for the analysis of the results, periods of 200 s were extracted by Yee and Biltoft (2004). These periods were indeed quasi-steady in terms of wind speed and direction and also remained greater than the plume travel time.

3.2. Description of the cases studied

As previously mentioned, the MUST experiment consisted of 63 tracer releases and in the work of Milliez and Carissimo (2007, 2008), twenty cases were simulated. In this work, we have chosen to study the trials 2681829 and 2092157, respectively corresponding to situations of neutral and stable atmospheres. The characteristics of these trials are summarized in Table 1, and the characteristics of all cases can be found in Milliez and Carissimo (2007).

4. Numerical simulations

In this section, we present the methodology and results of the numerical simulations of trials 2681829 and 2692157 in *Code_Saturne*.

4.1. Simulation domain and mesh

The simulation domain is of dimensions 240 m (North-South) $\times$ 240 m (East-West) $\times$ 100 m (vertical direction). The corresponding mesh is displayed in Figure 3. It is refined near the ground and the obstacles, the horizontal resolution varying from 4 m to 0.6 m. The vertical resolution of the mesh increases gradually from 0.2 m near the ground until it reaches 4 m at the top of the domain. In total, the mesh contains 1 426 010 cells.

4.2. Numerical setup

4.2.1. Fluid phase

For the flow, the models $k-\epsilon$ et $R_{ij}-\epsilon$ (with simple gradient-diffusion hypothesis for the scalars) are used and will be further compared. The imposed boundary conditions are the following:

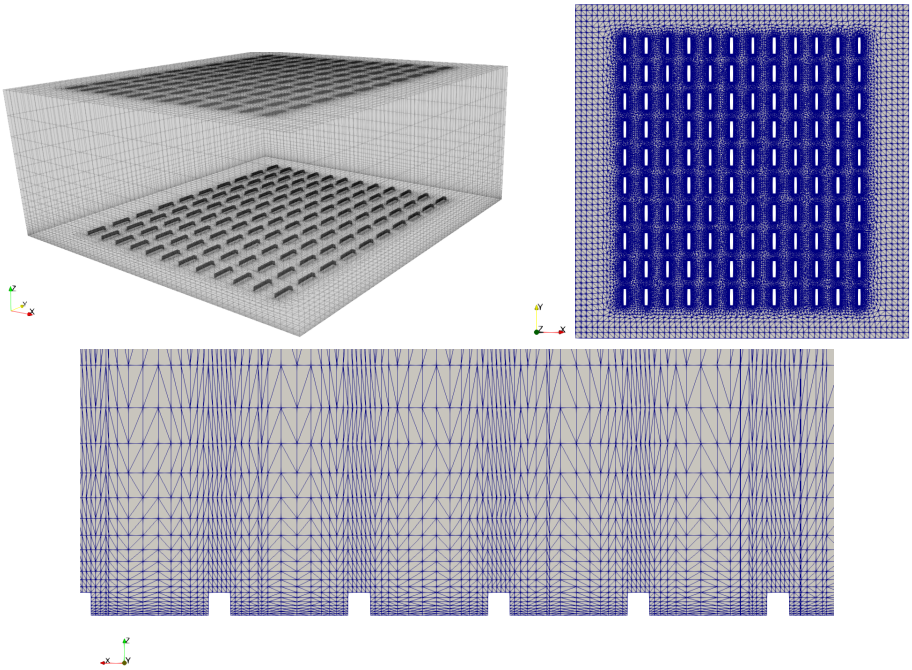

Figure 3: Mesh of the computational domain. From left to right and top to bottom: general view, horizontal cross-section, vertical cross-section.

- Inlet condition of Dirichlet type, with dynamical profiles derived from experimental measurements. Indeed, it has been shown in Milliez and Carissimo (2007) that the use of analytical profiles in equilibrium can induce an underestimation of turbulence. They found better results using experimental profiles (when available), which is why we have chosen to follow the same road.
- Outlet condition: free outflow.
- Ground and containers: rough wall, with a roughness length of 0.04 m.

4.2.2. Dispersed phase

With the Eulerian approach, the pollutant is injected through a scalar source term. At the injection cell, we have imposed a pollutant flow rate of 225 L/min for both neutral 2681829 and stable 2692157 trials (cf. Table 1). With the Lagrangian approach, at the same injection cell, 2 000 particles per time step are injected, with the same flow rate.

4.3. Results for neutral trial 2681829

4.3.1. Simulation of the fluid phase

As a reminder, we have performed two simulations of the fluid phase, corresponding respectively to the use of the first-order $k-\epsilon$ or second-order $R_{ij}-\epsilon$ turbulence closures. Figure 4 shows the mean velocity and TKE fields at height $z = 4\ m$ for both turbulence

models. This height stands above the roofs ($z_{roofs} = 2.54\ m$) and we can observe the influence of the row of containers on the flow. Naturally, a slowdown of the flow and an increase in turbulent kinetic energy can be observed. It can also be seen that $k-\epsilon$ model tends to predict higher levels of turbulent kinetic energy upstream of the obstacles, which is a well-known result in turbulence modeling. However, when comparing to the measurements, it can be seen that the TKE values are always underestimated, with both $k-\epsilon$ and $R_{ij}-\epsilon$ models. Figure 5 shows the wind field in the source area, at 1.6 m height: the recirculation zones between the containers are well-captured and explain the previously mentioned decrease of velocity above the roofs at 4 m height. The recirculation zones are also wider and more pronounced with the $R_{ij}-\epsilon$ model. Finally, we have plotted in Figure 6 the mean velocity and TKE vertical profiles extracted from the masts when data was available. Once again, turbulence production is more pronounced with $k-\epsilon$ model. Velocity profiles are on the other hand not much affected by the turbulence model (as is also seen in the velocity magnitude field of Figure 4) and stand in good agreement with the measurements.

4.3.2. Simulation of the dispersion

Figure 7 shows the concentration fields at height 1.6 m, for both $k-\epsilon$ and $R_{ij}-\epsilon$ models. Whether it be through the Eulerian or the Lagrangian approach, it can be observed that the choice of the turbulence model plays an important role on the concentration patterns. In particular, we can see that the plume is wider using the $R_{ij}-\epsilon$ model.

One can also observe that there is a deflection of the plume centerline compared to the -41^o wind direction. Note also that the plume deflection is more pronounced when using the $R_{ij}-\epsilon$ model, for both Eulerian and Lagrangian approaches. This deviation phenomenon has also been observed in Carissimo and Macdonald (2004) and Milliez and Carissimo (2007). Milliez and Carissimo (2007) explained it by the fact the pollutant is channeled into the streets perpendicular to the obstacle array axis, as is also observed in the experiment. Castelli et al. (2017), who also performed on the same trial Eulerian $k-\epsilon$ and Lagrangian calculations within their models RAMS6.0-mod and MicroRMS, noticed a lesser pronounced deflection with the Lagrangian modeling. They partly explained it by pointing out that their Lagrangian code did not account for the cross-correlation terms between the different components of wind velocity fluctuations. This is not the case with our model, since it is based on Pope's SLM, which implies that the cross-correlations of the wind velocity fluctuations are included in the mean-pressure gradient term of Eq. (3b) (this is actually one of the main advantages of this formulation, see Bahlali et al. (2018b) for more theoretical details). This may be why, when roughly comparing the concentration field obtained by Castelli et al. (2017) to the one we have displayed in Figure 7, we find a more pronounced deflection with the SLM than found in Castelli et al. (2017)'s results.

For a more precise analysis of the concentration field, we show in Figure 8 the concentration horizontal profiles on lines 1, 2, 3, 4 and in Figure 9 the vertical profiles on masts B, C, D and tower T. It can be observed that, in particular, the lines 1 and 2 show a shift in the plumes obtained by respectively the $k-\epsilon$ and the $R_{ij}-\epsilon$ models, which

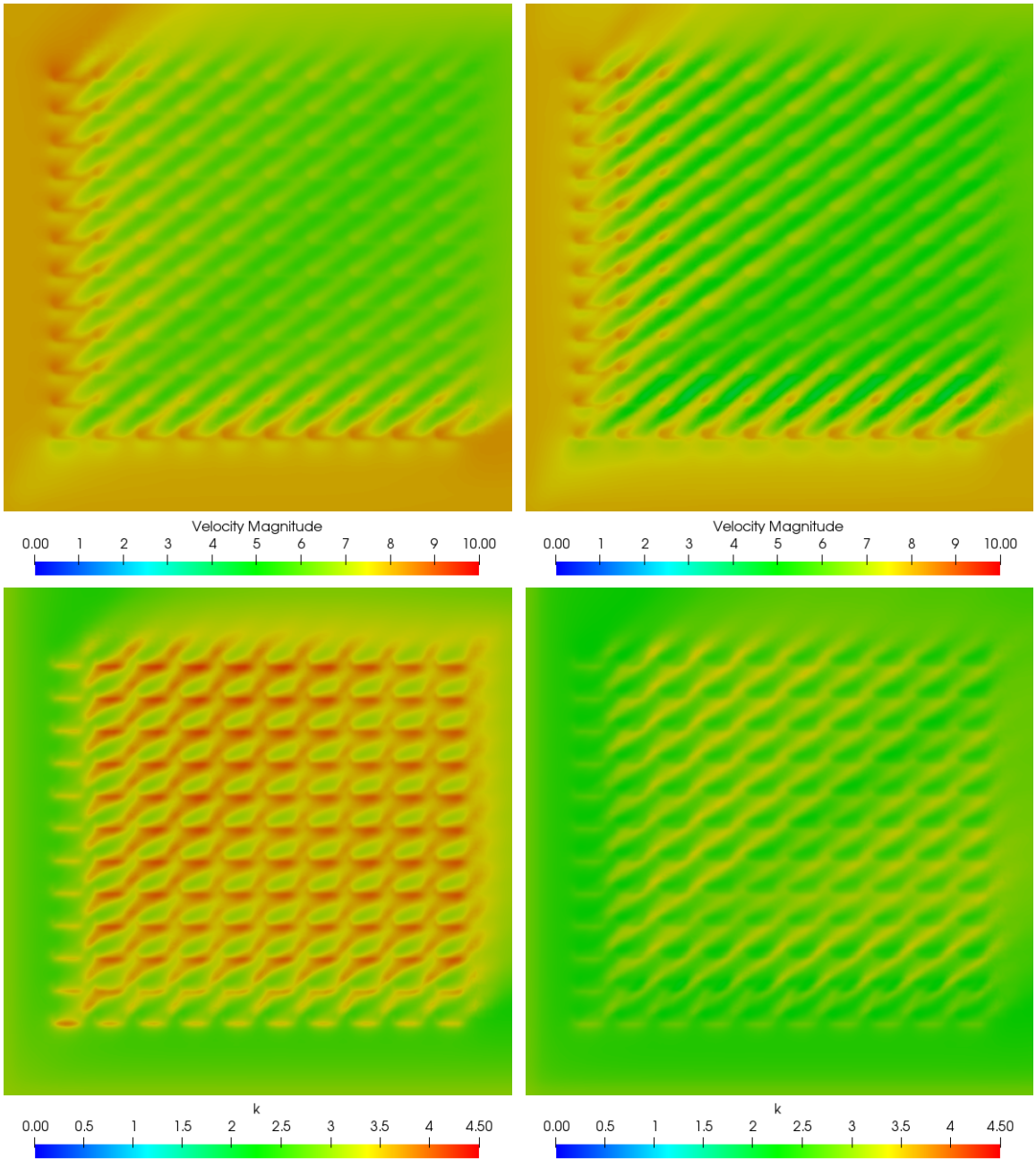

(a) $k - \epsilon$ model (b) $R_{ij} - \epsilon$ model

Figure 4: Comparison of mean velocity and TKE fields at $z = 4\ m$ computed by $k-\epsilon$ or $R_{ij}-\epsilon$ turbulence models, for neutral trial 2681829.

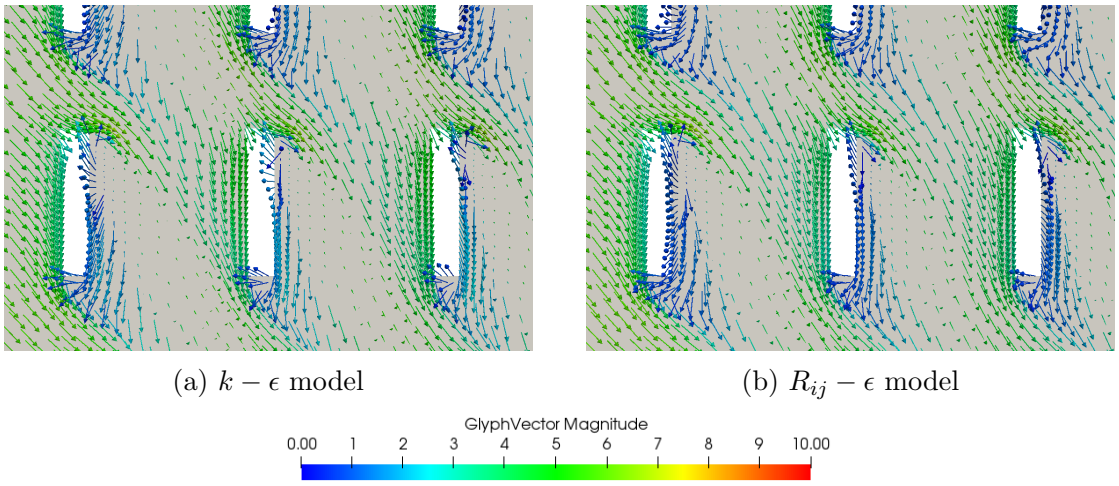

(a) $k - \epsilon$ model (b) $R_{ij} - \epsilon$ model

Figure 5: Comparison of wind fields around the source computed by $k - \epsilon$ or $R_{ij} - \epsilon$ turbulence models, for neutral trial 2681829.

again highlights the observed more pronounced deflection with the $R_{ij} - \epsilon$ closure. When using the $R_{ij} - \epsilon$ closure, the effect of the obstacles is clearly visible through the 'steps' corresponding to the regular spacing between the containers. If we compare Eulerian to Lagrangian results, it is interesting to have a look at the concentration evolution from line 1 (closest to the source) to line 4. Both models seem to have approximately the same evolution of diffusion. This is better seen in Figure 10, where we have plotted the maximum concentration value over each line against the distance from the source. It is well-known that Langevin-like Lagrangian models show rapid diffusion near the source and then tend to a diffusive law in the far-field. On the other hand, first-order Eulerian models based on a simple gradient diffusion hypothesis model the whole dispersion process through a diffusive law (which is actually a shortcoming of this kind of models since the gradient-diffusion hypothesis is no longer valid near the source). One then might wonder why, here in Figure 10, both Eulerian and Lagrangian models seem to show the same evolution of diffusion, independently from the distance to the source. In fact, one important thing to point out here is that line 1 is already located in the so-called 'far-field region'. Indeed, when speaking about near and far fields, it is always in comparison to the value of the Lagrangian integral timescale T_L. For small diffusion times with respect to the value of T_L, diffusion should be evolving proportionally to time, while for higher diffusion times, it should be evolving as square-root of time (Taylor, 1921). In our case, the value of T_L at the injection cell is 0.93 s, and the velocity norm is 4.5 $m.s^{-1}$, which yields a 'near-field region' of approximately $0.93 \times 4.5 = 4.2$ m. The far field is thus quickly reached. As the maximum concentration value on line 1 is located at approximately 60 m ($\gg 4.2$ m) from the source, we deduce by extension that all the lines are already in the well-established far-field region. In consequence, it is logical that both the Lagrangian and the Eulerian models show the same evolution of diffusion.

Apart from the previous remarks, and still analyzing the lines, the agreement between

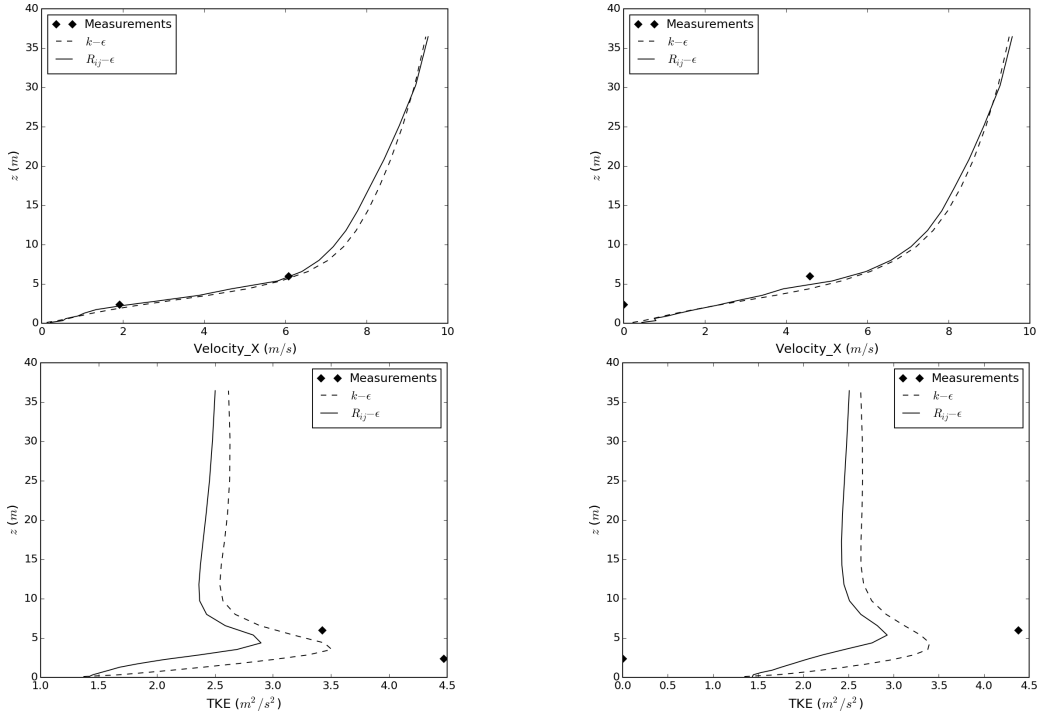

(a) Mast A

(b) Mast B

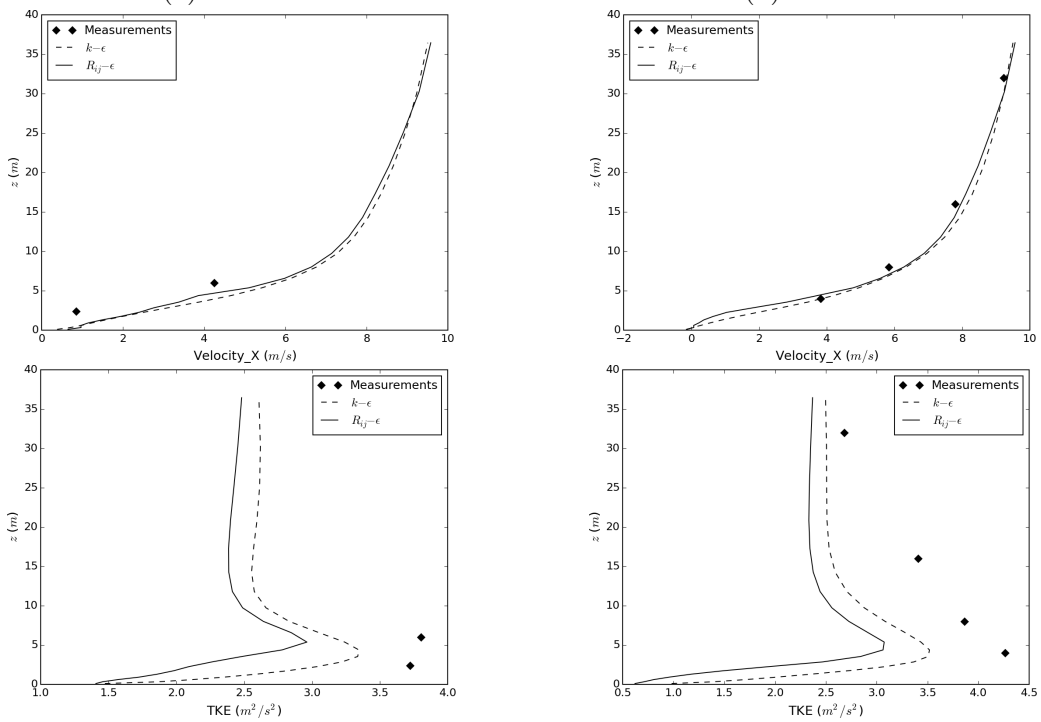

(c) Mast D

(d) Tower T

Figure 6: Comparison of vertical velocity and TKE profiles computed by $k-\epsilon$ or $R_{ij}-\epsilon$ turbulence models, for neutral trial 2681829.

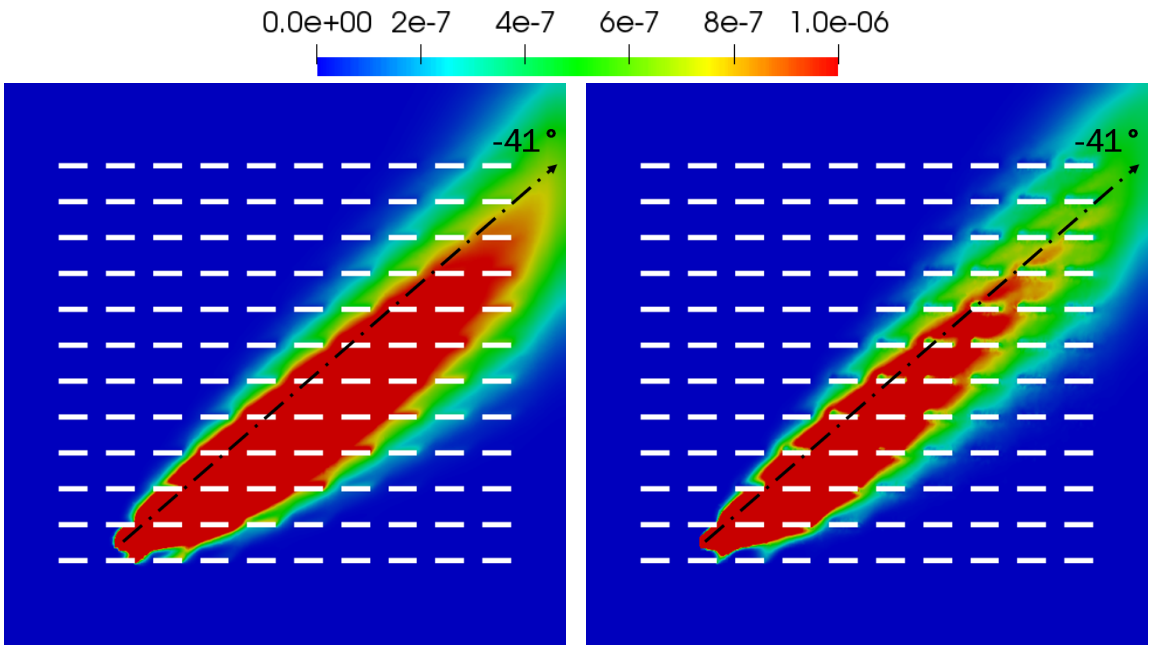

(a) Eulerian model, $k - \epsilon$

(b) Lagrangian model, $k - \epsilon$

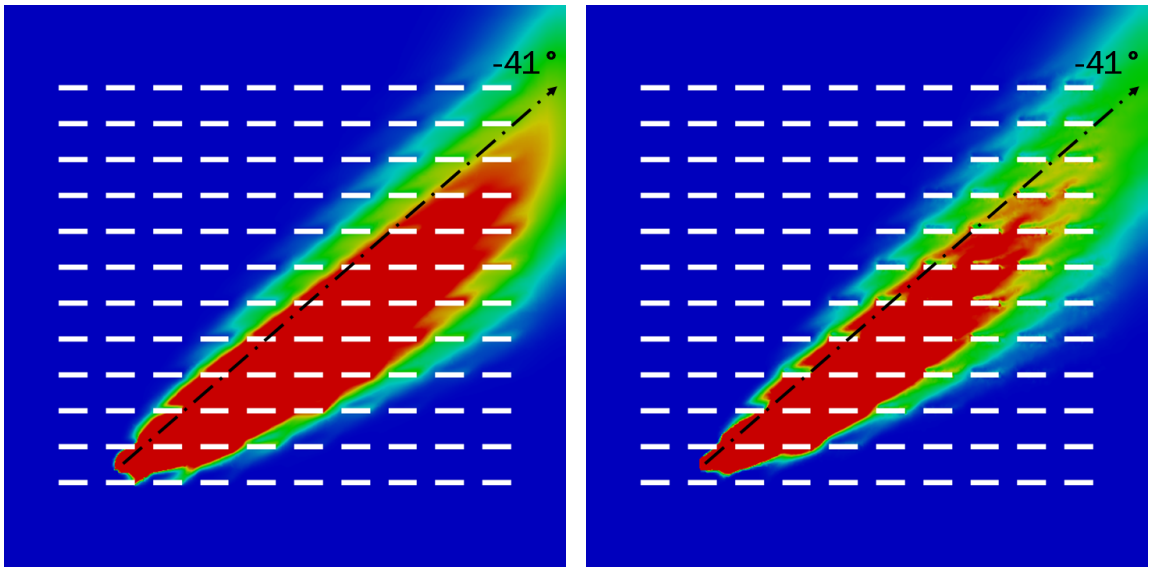

(c) Eulerian model, $R_{ij} - \epsilon$

(d) Lagrangian model, $R_{ij} - \epsilon$

Figure 7: Comparison of mean concentration (kg/kg) fields at $z = 1.6\ m$ computed by both Eulerian and Lagrangian models, through $k - \epsilon$ or $R_{ij} - \epsilon$ turbulence closures, for neutral trial 2681829.

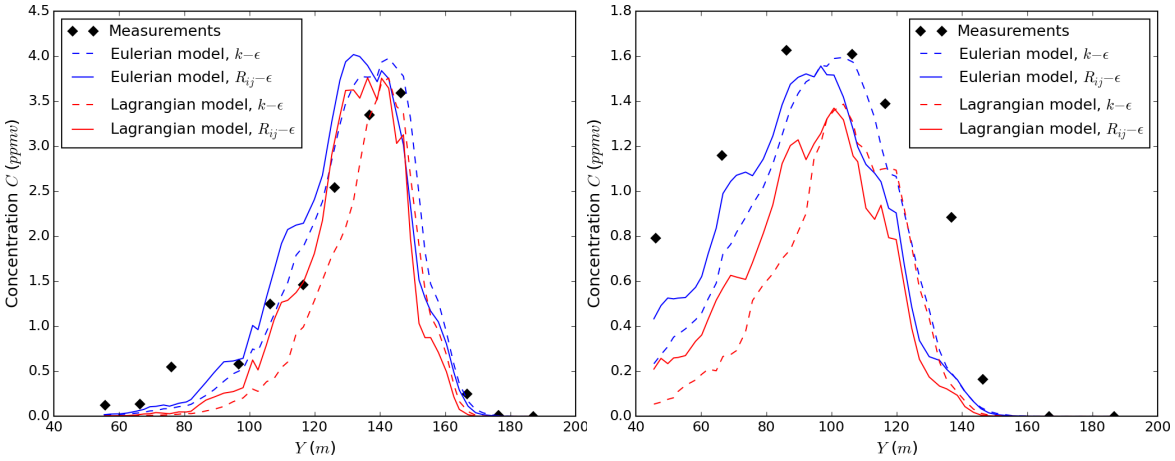

(a) Line 1

(b) Line 2

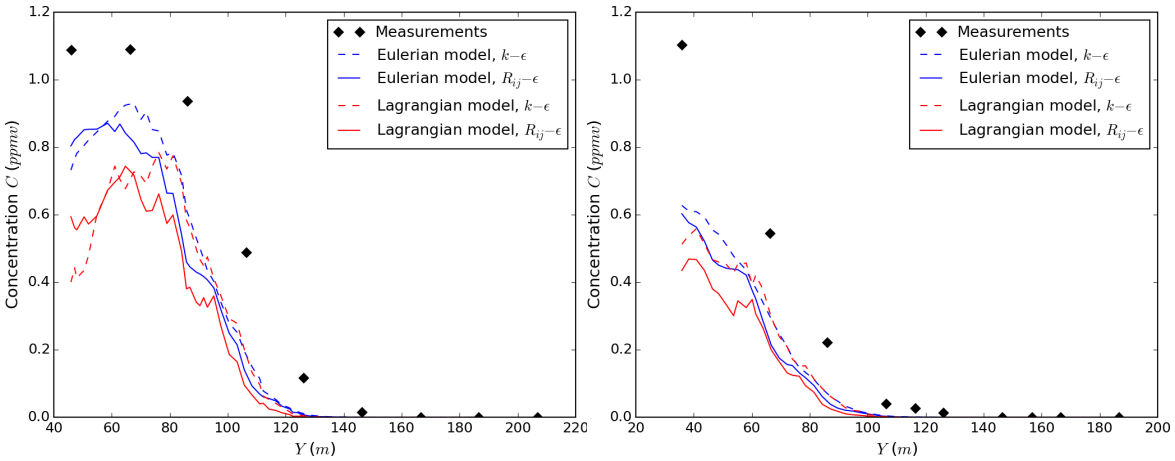

(c) Line 3

(d) Line 4

Figure 8: Comparison of concentration profiles on horizontal line samplers computed by both Eulerian and Lagrangian models, through $k-\epsilon$ or $R_{ij}-\epsilon$ turbulence closures, for neutral trial 2681829.

simulations and measurements is overall satisfactory and both Eulerian and Lagrangian models provide a quite acceptable representation of the spread of the plume, although the Lagrangian model seems to slightly underestimate the concentrations on all the lines.

If we focus now on vertical profiles (see Figure 9), it can be seen that the use of the $R_{ij}-\epsilon$ model for the fluid phase tends to reduce the maxima of concentrations on mast B (closest to the source), especially with the Lagrangian approach, making the results in better agreement with the measurements. On tower T, the maxima of concentrations are also lower and are due to the fact that the plume deflection is more pronounced using the $R_{ij}-\epsilon$ model for both Eulerian and Lagrangian approaches, making the plume go towards the South direction with more intensity and leaving lower concentration values on tower T. On mast C, the concentrations are also slightly reduced when using the $R_{ij}-\epsilon$ model for the same reason as for tower T. It is interesting to notice that on this mast, the Lagrangian

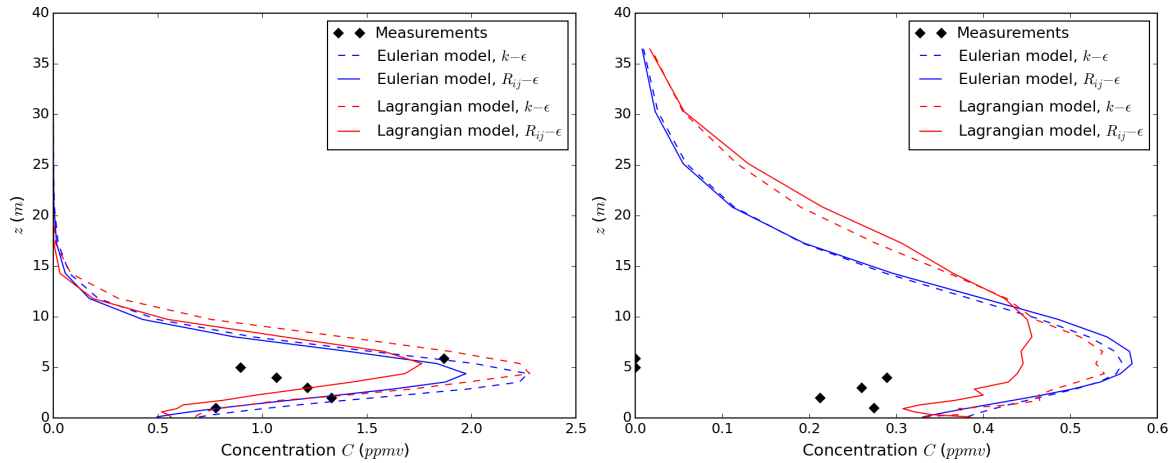

(a) Mast B

(b) Mast C

(c) Mast D

(d) Tower T

Figure 9: Comparison of vertical concentration profiles computed by both Eulerian and Lagrangian models, through $k-\epsilon$ or $R_{ij}-\epsilon$ turbulence closures, for neutral trial 2681829.

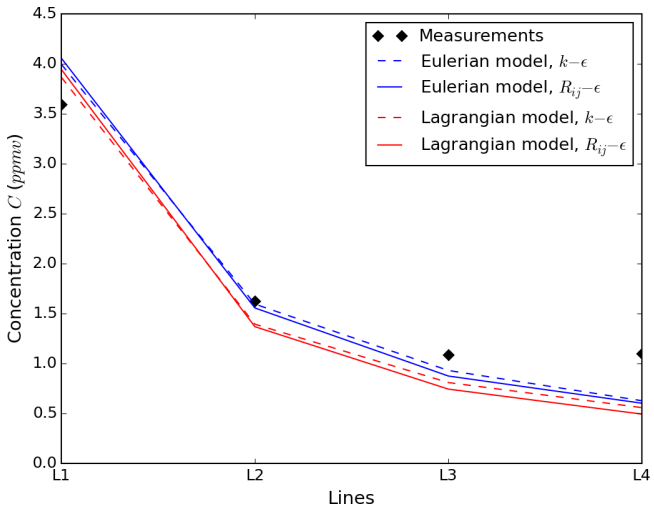

Figure 10: Maximum concentration value over each line against the distance from the source, for neutral trial 2681829.

approach captures the change of sign in the vertical gradient of concentration near the ground, while the Eulerian model does not. This is even more marked with the use of the $R_{ij} - \epsilon$ model. Finally, on mast D, concentrations are raised up when using the $R_{ij} - \epsilon$ model, which can also be explained by the plume deflection towards the South direction more pronounced with this model. On this mast, the Lagrangian approach provides better agreement with the measurements. However, note that one must be cautious in giving definite conclusions for masts C and D, since the concentrations are lower and can then imply more significant errors and uncertainties.

4.4. Results for stable trial 2692157

4.4.1. Simulation of the fluid phase

Analogously to neutral trial 2681829, we show in Figure 11 the mean velocity and TKE vertical profiles on masts A, B, C and tower T for both $k-\epsilon$ and $R_{ij}-\epsilon$ turbulence models. Velocities and TKE values are much lower than for trial 2681829, which is typical of stable stratification meteorological conditions. As in case 2681829, $k-\epsilon$ model tends to predict higher values of TKE than does $R_{ij}-\epsilon$ model. Velocity profiles are in good agreement with the measurements. Once again, they are not much affected by the choice of the turbulence model.

4.4.2. Simulation of the dispersion

Figure 12 displays the different concentration fields at height 1.6 m. It can be seen that as in trial 2681829, the plume is also wider when $R_{ij} - \epsilon$ model is used. The difference is even more pronounced through the Lagrangian approach. In addition, a plume deflection (compared to the 43^o wind direction) can also be observed in both Eulerian and Lagrangian results, more significant when using the $R_{ij} - \epsilon$ than the $k - \epsilon$ model for the fluid phase computation.

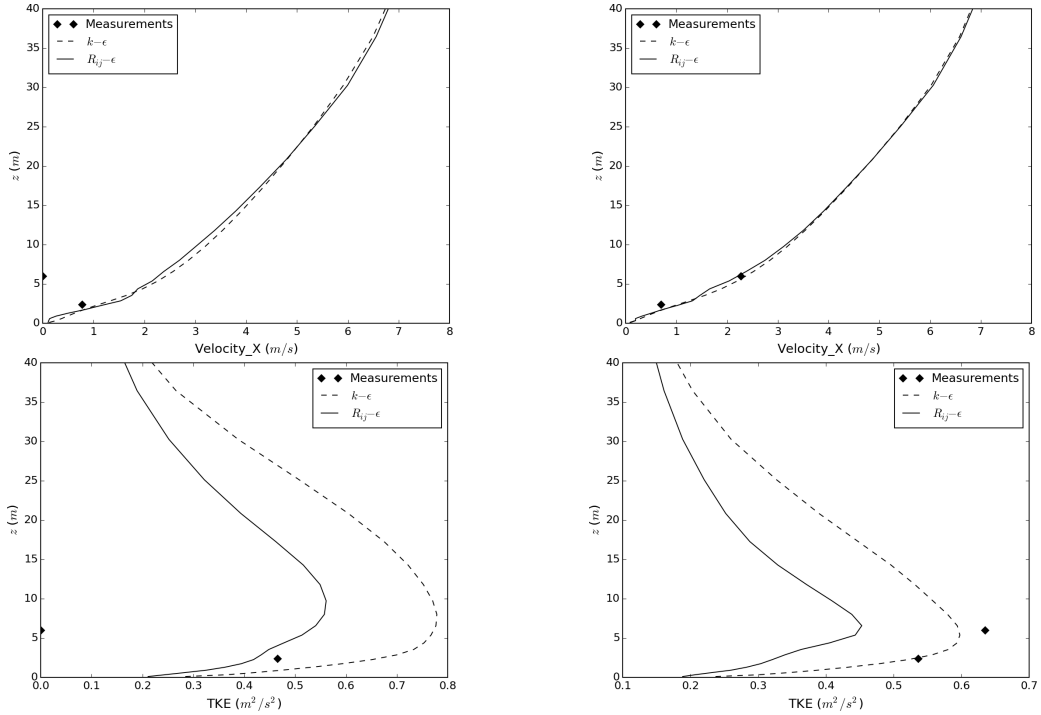

(a) Mast A

(b) Mast B

(c) Mast C

(d) Tower T

Figure 11: Comparison of vertical velocity and TKE profiles computed by $k-\epsilon$ or $R_{ij}-\epsilon$ turbulence models, for stable trial 2692157.

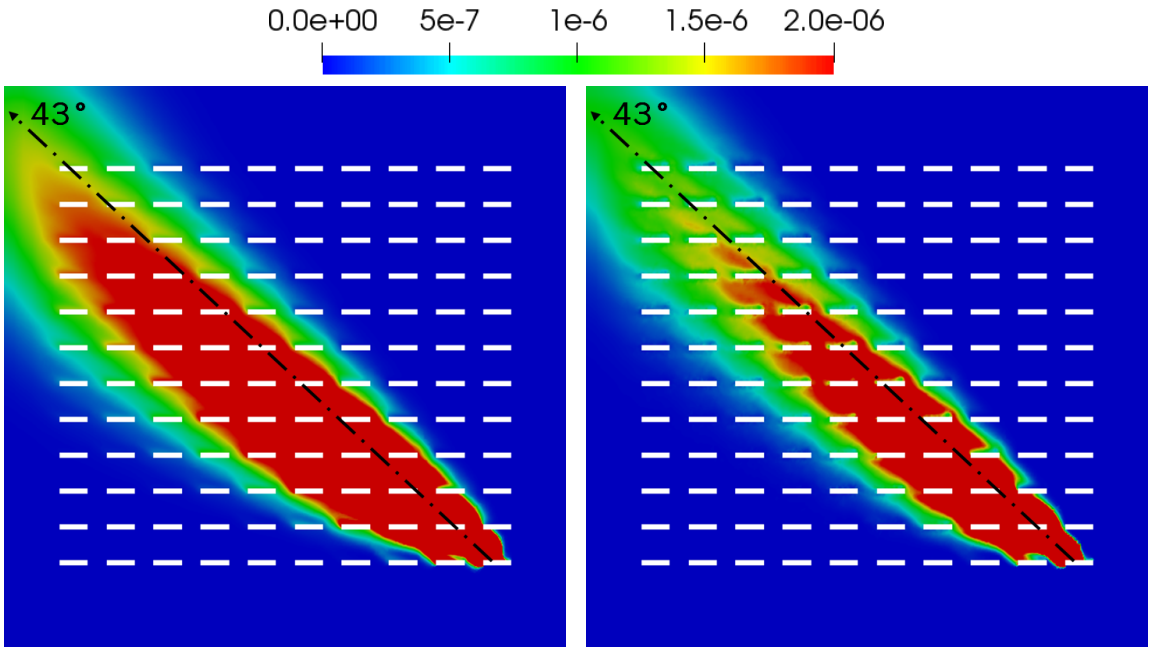

(a) Eulerian model, $k - \epsilon$

(b) Lagrangian model, $k - \epsilon$

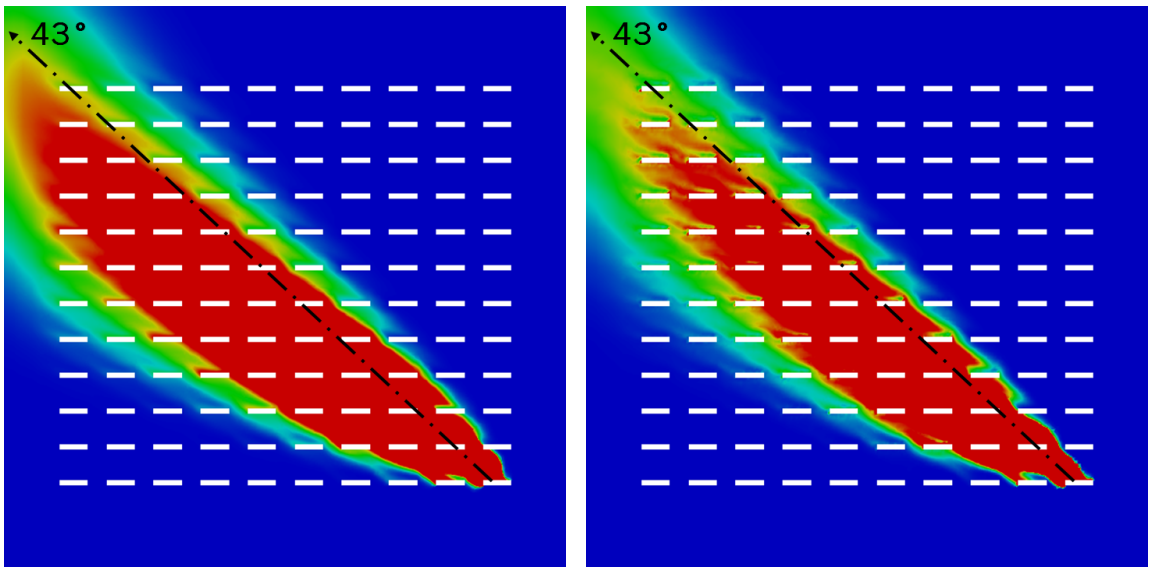

(c) Eulerian model, $R_{ij} - \epsilon$

(d) Lagrangian model, $R_{ij} - \epsilon$

Figure 12: Comparison of mean concentration (kg/kg) fields at $z = 1.6\ m$ computed by both Eulerian and Lagrangian models, through $k - \epsilon$ or $R_{ij} - \epsilon$ turbulence closures, for stable trial 2692157.

In Figure 13, we show the horizontal concentration profiles on lines 1, 2, 3 and 4. It can be seen that the use of the $R_{ij} - \epsilon$ model leads to an overprediction of concentrations on line 1, for both Eulerian and Lagrangian approaches, even more marked on the Eulerian results. Such an overprediction may be due to the fact that TKE is underestimated with the $R_{ij} - \epsilon$ model as seen in Figure 11. Nevertheless, the $R_{ij} - \epsilon$ model shows again the advantage of better capturing the presence of the obstacles through the visible regular concentration 'steps'. Regardless of the turbulence model, one can also notice the strong decrease of concentrations between line 1 and line 2 with both Lagrangian and Eulerian models, less marked when moving to the next lines: the evolution of diffusion induced by both models look similar. In this trial, at the injection cell, $T_L = 0.73\ s$ and the velocity equals $1.7\ m.s^{-1}$: in consequence, the region corresponding to the 'near field' corresponds to distances below $0.73 \times 1.7 = 1.2\ m$. The far field is thus immediately reached. Finally, one may notice that the further we walk from the source, the closer Eulerian and Lagragian curves stand to each other. Also, the agreement with experimental measurements rises up.

In Figure 14 are displayed the vertical concentration profiles on masts A, B, D and tower T. On mast D, which is the closest to the source, both Lagrangian and Eulerian models overpredict the concentrations when the $R_{ij} - \epsilon$ model is used. Nevertheless, when using the $k - \epsilon$ closure, both models provides very accurate results. Same goes for tower T, where the use of the $R_{ij} - \epsilon$ turbulence closure leads to an overprediction of concentration especially near the ground. On this mast, it is interesting to point out that even though the Lagrangian model used with the $k - \epsilon$ closure underpredicts the concentration values, it captures the change in the sign of the vertical concentration gradient near the ground. Stepping even further from the source and looking at mast A, one can notice a stronger vertical diffusion in the Lagrangian results. In this case again, concentrations are overpredicted. For this trial, the study of masts D, T and A is interesting as the 'D-T-A' parametrical line is roughly aligned with the centerline of the plume. One general conclusion from these three masts is that the use of the $R_{ij} - \epsilon$ model leads to an overprediction of concentrations especially near the ground. As for the concentrations on mast B, they are influenced by the plume deviation. Indeed, since the $R_{ij} - \epsilon$ model involves a more pronounced deflection of the plume than the $k-\epsilon$ model towards the West direction, where mast B is located, then concentrations are expected to be higher, which is indeed what is observed in the simulation results. However, and once again, better accuracy is found when the $k - \epsilon$ model is used for both Eulerian and Lagrangian approaches (except on mast B for the Lagrangian results).

From all these results on stable stratification, one may think that the tendency of the $k - \epsilon$ model to compute high TKE values can be seen as an 'advantage' for stable conditions, since this strengthens diffusion processes and thus leads to lower concentration values (that are, in general, and in particular looking at the lines, in better agreement with the measurements). In fact, one should remember here that even when using a $R_{ij} - \epsilon$ model, the closure on potential temperature is still local, through the following Generalized Gradient Diffusion Hypothesis (GGDH):

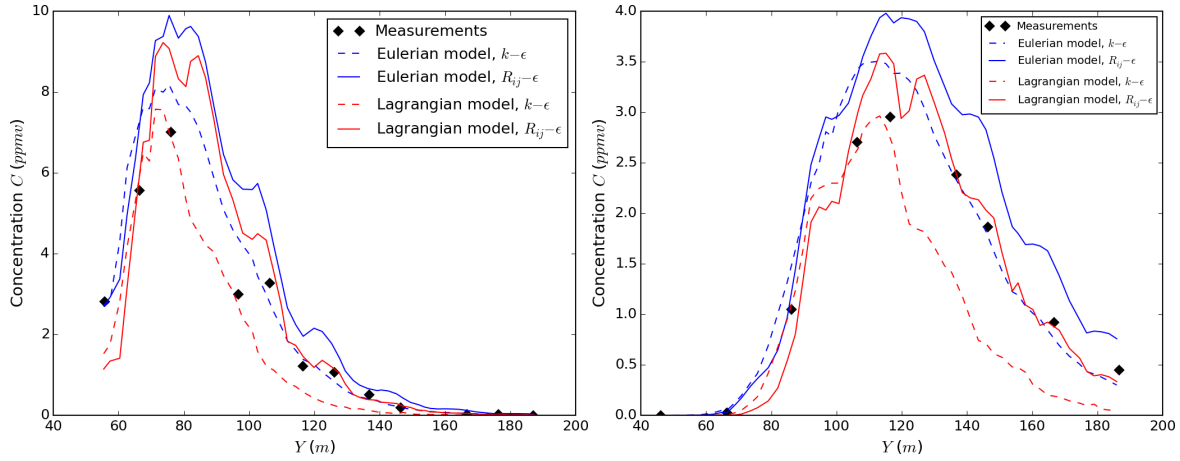

(a) Line 1

(b) Line 2

(c) Line 3

(d) Line 4

Figure 13: Comparison of concentration profiles on horizontal line samplers computed by both Eulerian and Lagrangian models, through $k-\epsilon$ or $R_{ij}-\epsilon$ turbulence closures, for stable trial 2692157.

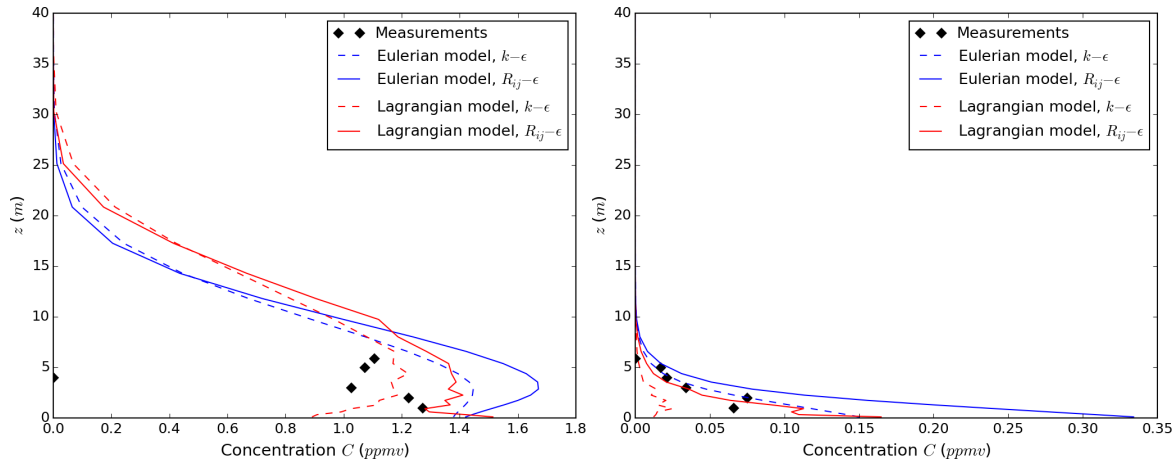

(a) Mast A

(b) Mast B

(c) Mast D

(d) Tower T

Figure 14: Comparison of vertical concentration profiles computed by both Eulerian and Lagrangian models, through $k-\epsilon$ or $R_{ij}-\epsilon$ turbulence closures, for stable trial 2692157.

$$\langle U'_{f,j}\theta'\rangle = -C_\theta \frac{k}{\epsilon}\left(\langle U'_{f,j}U'_{f,k}\rangle \frac{\partial\langle\theta\rangle}{\partial x_k}\right) \ , \tag{4}$$

where $C_\theta = 0.3$.

An improvement, still under investigation, could be the use of a second-order model on potential temperature.

5. Conclusions

This work aimed at assessing the ability of a Lagrangian stochastic model to perform point source dispersion in an idealized urban area, for neutral and stable meteorological conditions. The Lagrangian model used was a model based on Pope (2000)'s SLM and Minier and Peirano (2001)'s two-phase flow formulation. Pope's PDF models have gone quite unnoticed in the atmospheric dispersion community, despite presenting some non-negligible theoretical and numerical advantages (see Bahlali et al. (2018a,b)).

As used within a hybrid Eulerian/Lagrangian approach, the Lagrangian solver was fed by the mean dynamical fields provided by the Eulerian solver of the same CFD code *Code_Saturne*. These fields were computed either through a first-order $k-\epsilon$ model or a second-order $R_{ij}-\epsilon$ model. The Lagrangian results were compared to the Eulerian ones, for both turbulence models. The Eulerian turbulence closure for the scalar fluctuations was first order, which implied constant diffusivity. We showed that since the region considered for concentration measurements is already located in the far field (*i.e.*, diffusion times higher than the Lagrangian integral timescale), both Eulerian and Lagrangian show the same evolution of diffusion.

Then, we showed that the obstacle array induced a deflection of the plume, as already observed by Milliez and Carissimo (2007) in the same code and Castelli et al. (2017) in another methodology. These works modeled turbulence only through a $k-\epsilon$ closure. Precisely, we showed that this plume deflection was more pronounced using a $R_{ij}-\epsilon$ model. This was the case with both Eulerian and Lagrangian approaches. For neutral stratification, the agreement between results and measurements is quite satisfactory. In particular, we can validate the accuracy of the results of the Lagrangian model. We showed that the use of the $R_{ij}-\epsilon$ model made it possible to have a more physical representation of the obstacles' influence on the concentration profiles, through the visible regular 'steps' corresponding to the spacing between the containers.

For stable stratification, we showed that the results obtained by both approaches were more accurate when using a $k-\epsilon$ closure for the fluid phase. Not as satisfactory results as for neutral trial were found with the use of the $R_{ij}-\epsilon$ closure for stable stratification. The Lagrangian model, which is dependent on the quality of the flow calculated by the Eulerian solver, also see its results affected by the use of the $R_{ij}-\epsilon$ model. Deeper investigations are needed on this subject, but it should be noted that the temperature fluctuations closure is still local even with the $R_{ij}-\epsilon$ model. For further investigations, an idea would be to explore full second-moment closure modeling for both temperature and scalar fluctuations.

In the Lagrangian modeling, another research path would be to add a temperature scalar to the state vector of the particles, driven by a new stochastic differential equation (in the spirit of the works of Das and Durbin (2005) or Bossy et al. (2018) for instance), in order to better account for buoyancy-induced turbulent patterns.

References

Alessandrini, S., Ferrero, E., 2009. A hybrid Lagrangian–Eulerian particle model for reacting pollutant dispersion in non-homogeneous non-isotropic turbulence. Physica A: Statistical Mechanics and its Applications 388 (8), 1375–1387.

Amicarelli, A., Leuzzi, G., Monti, P., et al., 2012. Lagrangian micromixing models for concentration fluctuations: an overview. American Journal of Environmental Sciences 8 (6), 577–590.

Antonioni, G., Burkhart, S., Burman, J., Dejoan, A., Fusco, A., Gaasbeek, R., Gjesdal, T., Jäppinen, A., Riikonen, K., Morra, P., et al., 2012. Comparison of CFD and operational dispersion models in an urban-like environment. Atmospheric Environment 47, 365–372.

Archambeau, F., Méchitoua, N., Sakiz, M., 2004. Code Saturne: A finite volume code for the computation of turbulent incompressible flows-Industrial applications. International Journal on Finite Volumes 1 (1), http://code–saturne.org.

Bahlali, M. L., Dupont, E., Carissimo, B., 2018a. A hybrid CFD RANS/Lagrangian approach to model atmospheric dispersion of pollutants in complex urban geometries. Submitted to International Journal of Environment and Pollution.

Bahlali, M. L., Henry, C., Carissimo, B., Minier, J.-P., 2018b. On the well-mixed condition and consistency issues in hybrid Eulerian/Lagrangian stochastic models of dispersion. Submitted to Atmospheric Environment.

Bernardin, F., Bossy, M., Chauvin, C., Drobinski, P., Rousseau, A., Salameh, T., 2009. Stochastic downscaling method: application to wind refinement. Stochastic Environmental Research and Risk Assessment 23 (6), 851–859.

Biltoft, C. A., 2001. Customer report for Mock Urban Setting Test. DPG Document Number 8-CO-160-000-052. Prepared for the Defence Threat Reduction Agency.

Bossy, M., Dupré, A., Drobinski, P., Violeau, L., Briard, C., 2018. Stochastic Lagrangian approach for wind farm simulation, http://hal.inria.fr/hal–01697815/.

Camelli, F., Lohner, R., Hanna, S., 2005. VLES study of MUST experiment. In: 43rd AIAA Aerospace Sciences Meeting and Exhibit. p. 1279.

Carissimo, B., Macdonald, R., 2004. A porosity/drag approach for the modeling of flow and dispersion in the urban canopy. In: Air Pollution Modeling and Its Application XV. Springer, pp. 385–393.

Cassiani, M., Franzese, P., Giostra, U., 2005a. A PDF micromixing model of dispersion for atmospheric flow. Part I: development of the model, application to homogeneous turbulence and to neutral boundary layer. Atmospheric Environment 39 (8), 1457–1469.

Cassiani, M., Franzese, P., Giostra, U., 2005b. A PDF micromixing model of dispersion for atmospheric flow. Part II: application to convective boundary layer. Atmospheric Environment 39 (8), 1471–1479.

Cassiani, M., Stohl, A., Brioude, J., 2015. Lagrangian Stochastic Modelling of Dispersion in the Convective Boundary Layer with Skewed Turbulence Conditions and a Vertical Density Gradient: Formulation and Implementation in the FLEXPART Model. Boundary-Layer Meteorology 154 (3), 367–390.

Castelli, S. T., Tinarelli, G., Reisin, T., 2017. Comparison of atmospheric modelling systems simulating the flow, turbulence and dispersion at the microscale within obstacles. Environmental Fluid Mechanics 17 (5), 879–901.

Das, S., Durbin, P. A., 2005. A Lagrangian stochastic model for dispersion in stratified turbulence. Physics of Fluids 17 (2), 025109.

Dejoan, A., Santiago, J., Martilli, A., Martin, F., Pinelli, A., 2010. Comparison between Large-Eddy Simulation and Reynolds-averaged Navier–Stokes computations for the MUST field experiment. Part II: effects of incident wind angle deviation on the mean flow and plume dispersion. Boundary-Layer Meteorology 135 (1), 133–150.

Donnelly, R., Lyons, T., Flassak, T., 2009. Evaluation of results of a numerical simulation of dispersion in an idealised urban area for emergency response modelling. Atmospheric Environment 43 (29), 4416–4423.

Franzese, P., 2003. Lagrangian stochastic modeling of a fluctuating plume in the convective boundary layer. Atmospheric Environment 37 (12), 1691–1701.

Hanna, S. R., Hansen, O. R., Dharmavaram, S., 2004. FLACS CFD air quality model performance evaluation with Kit Fox, MUST, Prairie Grass, and EMU observations. Atmospheric Environment 38 (28), 4675–4687.

Kumar, P., Feiz, A.-A., Ngae, P., Singh, S. K., Issartel, J.-P., 2015. CFD simulation of short-range plume dispersion from a point release in an urban like environment. Atmospheric Environment 122, 645–656.

Leitl, B., Bezpalcova, K., Harms, F., 2007. Wind tunnel modelling of the MUST experiment. In: Proceeding of the 11th International Conference on Harmonization within Atmospheric Dispersion Modelling for Regulatory Purposes, Cambridge. Vol. 2. p. 435e439.

Luhar, A. K., Sawford, B. L., 2005. Micromixing modelling of concentration fluctuations in inhomogeneous turbulence in the convective boundary layer. Boundary-Layer Meteorology 114 (1), 1–30.

Milliez, M., 2006. Modélisation micro-météorologique en milieu urbain: dispersion des polluants et prise en compte des effets radiatifs. Ph.D. thesis, École nationale des ponts et chaussées (France).

Milliez, M., Carissimo, B., 2007. Numerical simulations of pollutant dispersion in an idealized urban area, for different meteorological conditions. Boundary-Layer Meteorology 122 (2), 321–342.

Milliez, M., Carissimo, B., 2008. Computational fluid dynamical modelling of concentration fluctuations in an idealized urban area. Boundary-Layer Meteorology 127 (2), 241–259.

Minier, J.-P., 2015. On Lagrangian stochastic methods for turbulent polydisperse two-phase reactive flows. Progress in Energy and Combustion Science 50, 1–62.

Minier, J.-P., 2016. Statistical descriptions of polydisperse turbulent two-phase flows. Physics Reports 665, 1–122.

Minier, J.-P., Chibbaro, S., Pope, S. B., 2014. Guidelines for the formulation of Lagrangian stochastic models for particle simulations of single-phase and dispersed two-phase turbulent flows. Physics of Fluids (1994-present) 26 (11), 113303.

Minier, J.-P., Peirano, E., 2001. The PDF approach to turbulent polydispersed two-phase flows. Physics Reports 352 (1), 1–214.

Pope, S., 1998. The vanishing effect of molecular diffusivity on turbulent dispersion: implications for turbulent mixing and the scalar flux. Journal of Fluid Mechanics 359, 299–312.

Pope, S. B., 2000. Turbulent flows.

Santiago, J., Dejoan, A., Martilli, A., Martin, F., Pinelli, A., 2010. Comparison between Large-Eddy Simulation and Reynolds-averaged Navier–Stokes computations for the MUST field experiment. Part I: study of the flow for an incident wind directed perpendicularly to the front array of containers. Boundary-Layer Meteorology 135 (1), 109–132.

Sawford, B., 2004. Micro-mixing modelling of scalar fluctuations for plumes in homogeneous turbulence. Flow, Turbulence and Combustion 72 (2-4), 133–160.

Stohl, A., Forster, C., Frank, A., Seibert, P., Wotawa, G., 2005. The Lagrangian particle dispersion model FLEXPART version 6.2. Atmospheric Chemistry and Physics 5 (9), 2461–2474.

Taylor, G. I., 1921. Diffusion by continuous movements. Proceedings of the London Mathematical Society 20, 196–211.

Thomson, D., 1987. Criteria for the selection of stochastic models of particle trajectories in turbulent flows. Journal of Fluid Mechanics 180, 529–556.

Tinarelli, G., Mortarini, L., Castelli, S. T., Carlino, G., Moussafir, J., Olry, C., Armand, P., Anfossi, D., 2013. Review and validation of MicroSpray, a Lagrangian particle model of turbulent dispersion. Lagrangian Modeling of the Atmosphere, 311–328.

Villermaux, J., Devillon, J., 1972. Représentation de la coalescence et de la redispersion des domaines de ségrégation dans un fluide par un modele dinteraction phénoménologique. In: Proceedings of the 2nd International Symposium on Chemical Reaction Engineering. Vol. 26. Elsevier New York, pp. 1–13.

Yee, E., Biltoft, C. A., 2004. Concentration fluctuation measurements in a plume dispersing through a regular array of obstacles. Boundary-Layer Meteorology 111 (3), 363–415.

Yee, E., Gailis, R. M., Hill, A., Hilderman, T., Kiel, D., 2006. Comparison of wind-tunnel and water-channel simulations of plume dispersion through a large array of obstacles with a scaled field experiment. Boundary-Layer Meteorology 121 (3), 389–432.

7.2 Complément

Ce paragraphe a pour objectif de réaliser une étude de sensibilité au nombre de particules, analoguement à notre étude du SIRTA (cf. chapitre 6). La procédure suivie est la même que celle suivie dans cette étude : nous sommes partis d'un nombre de particules conséquent afin d'assurer une bonne précision de nos calculs, puis nous avons souhaité observer l'influence de la diminution du nombre de particules sur la précision des résultats et le temps de calcul CPU.

Pour cette étude de sensibilité, nous avons sélectionné le cas neutre 2681829, avec la phase fluide calculée via le modèle $k-\epsilon$. Dans la simulation de ce cas présentée dans l'article Bahlali et al. (2018b), nous injections $N = 52\,000$ particules par seconde, pour un nombre total de 1 965 579 particules dans le domaine en fin de calcul. En plus de cette simulation, nous avons réalisé trois simulations supplémentaires, correspondant respectivement à : $N = 26\,000$, $N = 13\,000$ et $N = 4\,000$ particules injectées par seconde. Les nombres totaux de particules dans l'ensemble du domaine pour chacun de ces cas sont résumés en Table 7.1.

Pour réaliser nos comparaisons entre simulations, nous avons arbitrairement choisi une ligne et un mât de l'expérience : en l'occurrence, la ligne 3 et la tour T. Dans la Figure 7.1, nous montrons donc les profils obtenus pour l'ensemble des nouvelles simulations sur la ligne 3 et la tour T. A noter que dans chacune des sous-figures de la Figure 7.1, nous avons reproduit les profils correspondant aux résultats initialement obtenus avec $N = 52\,000$ particules injectées par seconde.

Nous observons des résultats très similaires entre $N = 52\,000$ et $N = 26\,000$ (Figures 7.1a et 7.1b), avec une très légère augmentation du bruit visible sur le profil relatif à la tour T (cf. Figure 7.1b). Au passage à $N = 13\,000$ (Figures 7.1c et 7.1d), l'augmentation du bruit est plus visible mais reste minime : ce cas pourrait tout à fait être exploitable dans un cadre opérationnel. En revanche, pour $N = 4\,000$ (Figures 7.1e et 7.1f), les courbes se dégradent et le bruit devient prédominant, en particulier sur la ligne 3 (cf. Figure 7.1e) : ces résultats ne sont pas exploitables.

En ce qui concerne les temps de calcul CPU, analoguement au cas du SIRTA en chapitre 6, nous avons tracé le graphe de la fonction reliant le temps de calcul CPU au nombre de particules simulées. Ce graphe est présenté en Figure 7.2. De même que pour le cas du SIRTA, nous observons un gain conséquent en temps de calcul pour les N grands, avec des gradients importants. Au fur et à mesure que N diminue, les gradients s'amenuisent et la réduction du nombre de particules devient ainsi moins intéressante vis-à-vis du temps de calcul CPU. Nous pouvons donc conclure, au vu de la bonne précision du calcul à $N = 13\,000$ (cf. Figures 7.1c et 7.1d) et du gain conséquent en

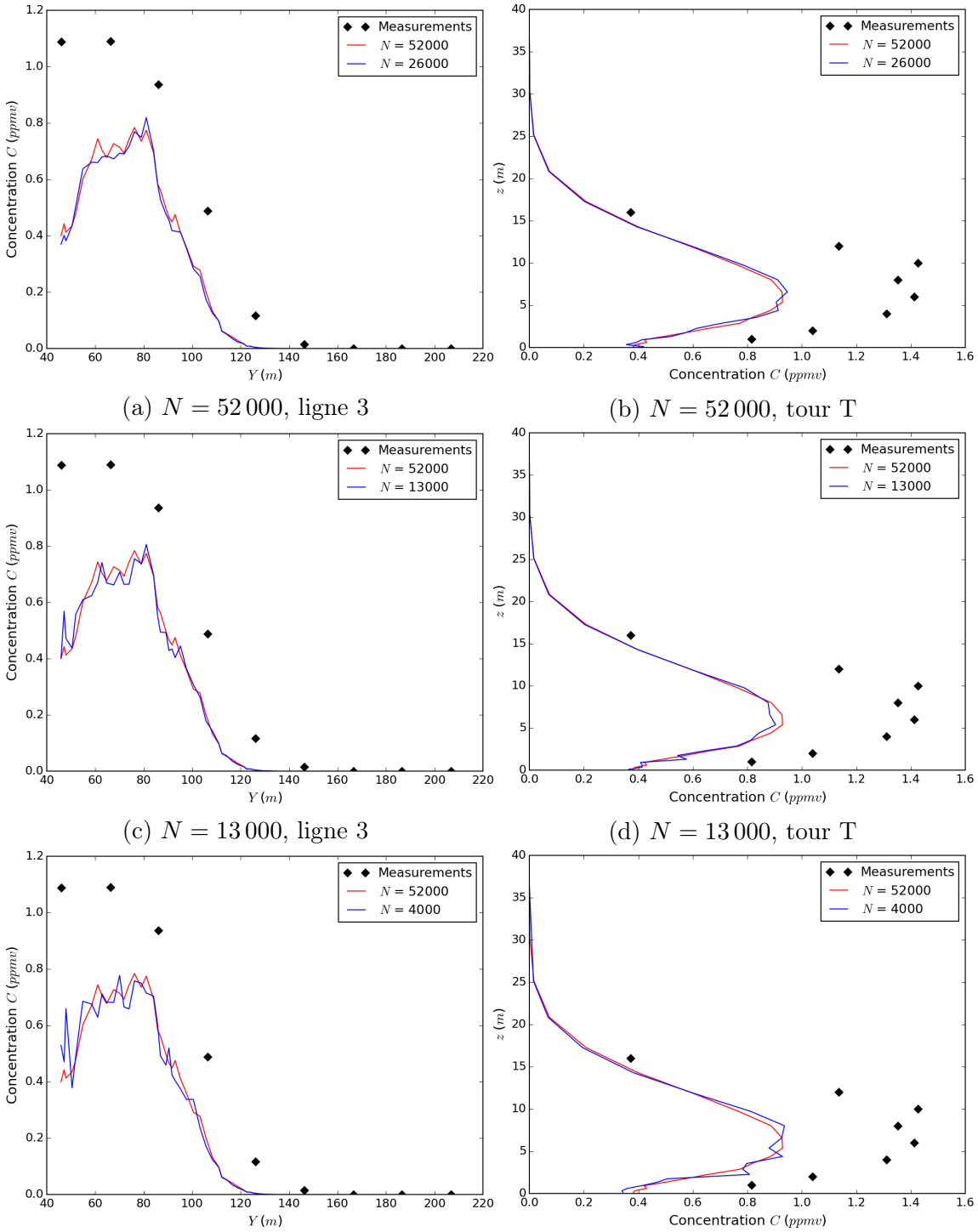

(a) $N = 52\,000$, ligne 3

(b) $N = 52\,000$, tour T

(c) $N = 13\,000$, ligne 3

(d) $N = 13\,000$, tour T

(e) $N = 4\,000$, ligne 3

(f) $N = 4\,000$, tour T

FIGURE 7.1 – Comparaison des profils de concentration (*ppmv*) sur les ligne 3 et tour T (cf. Figure 2 de l'article BAHLALI et al. (2018b)), en fonction du nombre de particules injectées par seconde N.

N	52 000	26 000	13 000	4 000
N_{total}	1 965 702	982 547	491 709	151 078

TABLE 7.1 – Résumé des simulations réalisées et des nombres de particules correspondants. N est le nombre de particules injectées par seconde, et N_{total} est le nombre de particules dans le domaine en fin de calcul.

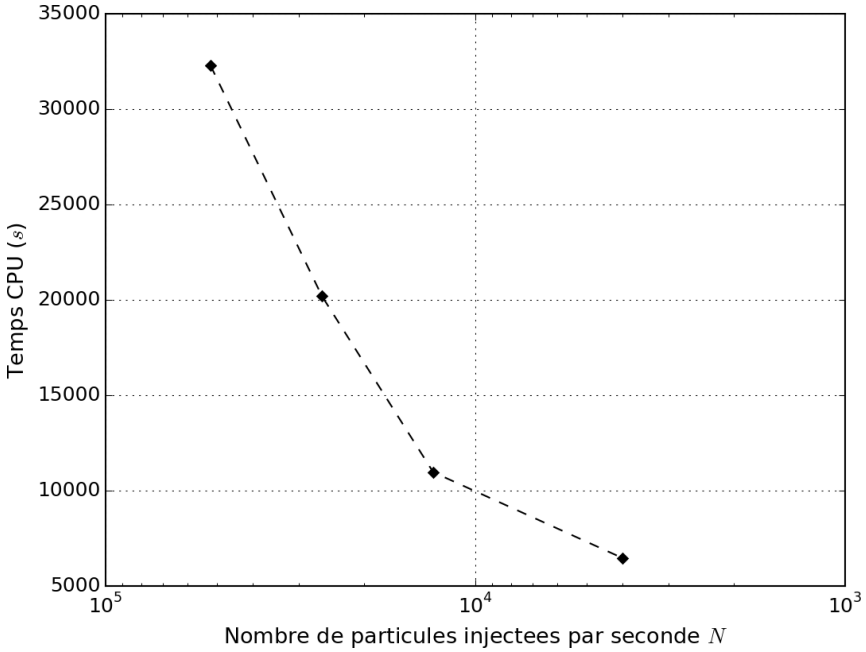

FIGURE 7.2 – Temps CPU (s) en fonction du nombre de particules injectées par seconde N, pour le cas neutre 2681829 de l'expérience MUST, avec un modèle $k - \epsilon$.

temps de calcul par rapport au cas initial à $N = 52\,000$ (nombre de particules divisé par 4 et temps de calcul divisé par 2.9), que cette option représente un bon compromis d'un point de vue opérationnel.